

# Thermodynamic Study of Interactions between ZnO and ZnO Binding Peptides Using Isothermal Titration Calorimetry

Marion J. Limo and Carole C. Perry\*

Biomolecular and Materials Interface Research Group, Interdisciplinary Biomedical Research Centre, School of Science and Technology, Nottingham Trent University, Clifton Lane, Nottingham, NG11 8NS, U.K.

---

**ABSTRACT:** Whilst material specific peptide binding sequences have been identified using a combination of combinatorial methods and computational modelling tools, a deep molecular level understanding of the fundamental principles through which these interactions occur and in some instances modify the morphology of inorganic materials is far from being fully realized. Understanding the thermodynamic changes that occur during peptide-inorganic interactions and correlating these to structural modifications of the inorganic materials could be the key to achieving and mastering control over material formation processes. This study is a detailed investigation applying isothermal titration calorimetry (ITC) to directly probe thermodynamic changes that occur during interaction of ZnO binding peptides (ZnO-BPs) and ZnO. The ZnO-BPs used are reported sequences G-12 (GLHVMHKVAPPR), GT-16 (GLHVMHKVAPPR-GGGC) and alanine mutants of G-12 (G-12A6, G-12A11 and G-12A12) whose interaction with ZnO during solution synthesis studies have been extensively investigated. The interactions of the ZnO-BPs with ZnO yielded biphasic isotherms comprising both an endothermic and an exothermic event. Qualitative differences were observed in the isothermal profiles of the different peptides and ZnO particles studied. Measured  $\Delta G$  values were between -6 and -8.5 kcal/mol and high adsorption affinity values indicated the occurrence of favourable ZnO-BP-ZnO interactions. ITC has great potential in its use to understand peptide-inorganic interactions and with continued development, the knowledge gained may be instrumental for simplification of selection processes of organic molecules for the advancement of material synthesis and design.

---

## INTRODUCTION

Following biomimetic strategies, there is an increasing body of evidence demonstrating that combinatorially selected material binding peptides such as those identified using phage display (PD) and post selection tailored peptides are able to control the morphology of non-biological inorganic materials.<sup>1-11</sup> Peptides have also been shown to act as stabilizers, reducing agents, catalysts or inhibitors when incorporated in solution syntheses of inorganic materials.<sup>10,12,13</sup> Great prospects lie in the use of material binding peptides to improve artificial material formation processes following more environmentally sustainable bio-inspired methods. The specificity between inorganic crystal surfaces and material binding peptides and the exact mechanisms of their interaction are however not clearly understood.<sup>3,6,14</sup> In biomineralization processes, where minerals are produced by living organisms, it is thought that biomolecules may control mineral formation by modification of the energy barriers at the interface.<sup>3,15</sup> Similarly, there may be a direct link between thermodynamic changes that occur at the peptide-inorganic interface and peptide-directed structural modification of inorganic materials. Therefore, understanding the energetic changes that occur during peptide-inorganic interactions and correlating these to structural modifications of the inorganic materials could be the key to advancing material synthesis/design and may also reveal key principles

through which material structure is controlled in nature.<sup>15-17</sup>

Of specific interest, in-house studies have been carried out to understand the fundamental principles through which ZnO binding peptides (ZnO-BPs) interact with and modify ZnO growth process and morphology.<sup>6,8,18</sup> In a recent contribution, the mechanisms through which specific ZnO binding peptides (ZnO-BPs) interact with and modify the growth process and morphology of ZnO during solution synthesis was described.<sup>8</sup> The peptides used in the study were PD identified G-12 (GLHVMHKVAPPR) peptide, its derivative GT-16 (GLHVMHKVAPPR-GGGC) and alanine mutants of the G-12 peptide.<sup>1,8</sup> The mutants were selected on the basis of peptide stability calculated *in silico* i.e., molecular dynamics (MD) simulations were used to monitor the conformation and stability of mutants generated by single point substitution of alanine into each position in G-12 sequence.<sup>8</sup> The mutants selected were G-12A6 (GLHVM $\underline{A}$ KVAPPR) and G-12A11 (GLHVMHKVAP $\underline{A}$ R), determined to be more stable than G-12 peptide and G-12A12 (GLHVMHKVAP $\underline{P}$ A) found to be the most unstable sequence generated in solvated and non-solvated states.<sup>8</sup> When incorporated in ZnO synthesis using a reported  $Zn(NO_3)_2 \cdot 6H_2O$ -HMTA method,<sup>1</sup> G-12, G-12A11 and G-12A12 all adsorbed to ZnO rods decreasing the aspect ratio of the crystals in comparison to rods formed in the absence of peptide.<sup>8</sup> Uniquely, incorpora-

tion of G-12A6 peptide resulted in the formation of microsphere structures.<sup>8</sup> Using a different synthesis method, the ZnAc<sub>2</sub>-NH<sub>3</sub> system,<sup>19</sup> in comparison to G-12A6, G-12 had a greater ability to inhibit ZnO formation by stabilizing the intermediate product layered basic zinc acetate (LBZA).<sup>8</sup>

Herein, to extend our understanding, isothermal titration calorimetry (ITC) has been employed to directly probe thermodynamic changes during interaction of the aforementioned ZnO-BPs with ZnO. Few studies have kinetically and thermodynamically characterized the interaction of ZnO-PBs with ZnO surfaces. Adsorption studies of fluorescent labelled EM-12 (EAHVMHKVAPRP) peptide (as well as alanine mutants, random rotations and short segments/truncations of the EM-12 sequence) to ZnO have been reported.<sup>20,21</sup> Thermodynamic parameters of interaction were estimated from Langmuir adsorption isotherms and van't Hoff equations.<sup>20,21</sup> In the study reported by Yokoo and colleagues,<sup>20</sup> change in Gibbs free energy ( $\Delta G$ ) values of tagged ZnO-BPs were estimated to lie in-between -7.17 and -8.37 kcal/mol.<sup>20</sup> Interactions were seen to be enthalpy driven with the main contribution from  $\Delta H$  values.<sup>20</sup> The adsorption process was mainly attributed to hydrogen bonding and electrostatic interactions through charged residues of the peptides.<sup>20</sup> Nuclear magnetic resonance (<sup>1</sup>H NMR) has also been used to determine the binding affinity of two phage display identified ZnO-BPs (HSSHQPKGTNP and HHGHSPTSPQVR) for ZnO particles by determining the line broadening effects during interaction of the peptides with different concentrations of ZnO and assuming a 1.1 Langmuir binding model.<sup>22</sup> HHGHSPTSPQVR peptide was found to be the stronger binder for the ZnO substrate used.<sup>22</sup>

The applications of ITC continue to evolve from conventional biomolecular recognition reactions into diverse areas of interest in the medical/academic fields and industrial sector. An example is the developing use of ITC to study interactions between proteins/peptides and inorganic nanoparticles for biomedical applications.<sup>16,23-25</sup> Though the use of ITC to study biotic-abiotic interactions is in its infancy it has great potential as it does not require labelling or immobilization of the interacting components and more exceptionally, it can directly measure molar enthalpy of interaction and determine all thermodynamic parameters (enthalpy change ( $\Delta H$ ), entropy change ( $\Delta S$ ),  $K_A$  and  $\Delta G$ ) in a single experiment.<sup>26,27</sup> Using ITC, the interaction of the studied ZnO-BPs with ZnO is seen to be an energetically favourable process and is described to involve different events some of which may be occurring simultaneously *i.e.* peptide-solvent, substrate-solvent, peptide-surface, possible conformation changes between bound and free peptide states and peptide-peptide interactions.

## EXPERIMENTAL SECTION

**Materials.** Zinc nitrate hexahydrate (Zn(NO<sub>3</sub>)<sub>2</sub>·6H<sub>2</sub>O) and 1,3-hexamethylenetetramine (HMTA, C<sub>6</sub>H<sub>12</sub>N<sub>4</sub>) were purchased from Sigma Aldrich for ZnO synthesis. Materials for the synthesis of peptides were; Fmoc-protected amino acids and 2-(1H-benzotriazole-1-yl)-1,1,3,3-tetramethyluronium hexafluorophosphate (HBTU) purchased from CEM Corporation, amino acid-preloaded

Wang resins from Novabiochem, Piperazine, diisopropyl ethylamine (DIEA), thioanisole (TIS, C<sub>7</sub>H<sub>8</sub>S), trifluoroacetic acid (TFA, C<sub>2</sub>H<sub>3</sub>F<sub>3</sub>O<sub>2</sub>) and 3,6-dioxo-1,8-octanedithiol (DODT, C<sub>6</sub>H<sub>14</sub>O<sub>2</sub>S<sub>2</sub>) from Sigma Aldrich. All materials were used without any further treatment. Where required, distilled-deionized water (ddH<sub>2</sub>O) having conductivity measurement of less than 1  $\mu\text{S cm}^{-1}$  at 25 °C was used.

**Synthesis of Peptides and ZnO.** The synthesis and characterization of peptides and ZnO particles used in this study has previously been described in detail.<sup>8</sup> Peptides were synthesized *via* Fmoc chemistry using microwave assisted solid phase peptide synthesis technique (Liberty1 instrument CEM Corporation).<sup>8</sup> Peptide purity and molecular weight were ascertained using reverse phase high performance liquid chromatography (Dionex RP-HPLC) and matrix-assisted laser desorption/ionization time-of-flight mass spectrometry (Bruker Ultraflex III MALDI-TOF).<sup>8</sup> ZnO particles were synthesized following a method using Zn(NO<sub>3</sub>)<sub>2</sub>·6H<sub>2</sub>O and HMTA to form elongated twinned rods and a modification of the method incorporating GT-16 peptide to form lower aspect ratio ZnO twinned platelets.<sup>1,6,8</sup> Synthesized ZnO particles had been characterized using several techniques; scanning electron microscopy (JEOL JSM-840A SEM), Energy dispersive X-ray (EDX) analysis, X-ray diffraction (X'Pert PRO XRD), Fourier transform infrared spectroscopy (Nicolet Magna IR-750), and Thermogravimetric analysis (Mettler Toledo TGA/SDTA 851e).<sup>8</sup> Herein, additional characterization of the ZnO particles was carried out before ITC experiments. Raman spectroscopy (Nicolet iS50) was used to identify the functional groups present in the ZnO particles, specifically to characterize peptide adsorption to ZnO platelets. The surface chemical constituents of the ZnO platelets were identified using X-ray photoelectron spectroscopy (VG Scientific ESCALAB Mkii XPS) as previously described.<sup>28</sup> The surface area of ZnO was determined using a Quantachrome Monosorb nitrogen gas adsorption instrument and the single-point Brunauer-Emmett-Teller (BET) method. The surface area of the ZnO rods was determined to be 3.8 m<sup>2</sup>/g and the surface area of ZnO platelets synthesized using GT-16 was 4.2 m<sup>2</sup>/g. A dissolution study was conducted to confirm the reproducibility of ZnO sample preparation by Inductively coupled plasma atomic emission spectroscopy (ICP-OES, Perkin Elmer Optima 2100DV) quantification of the amount of Zn<sup>2+</sup> ions dissolved from ZnO suspensions prepared for ITC experiments. The concentration of Zn<sup>2+</sup> ions was determined to be 0.10 ± 0.01 mM. There was no significant difference (ANOVA, *p* value > 0.05, *n* = 21) in the amount of Zn<sup>2+</sup> ions present between samples prepared.

**ITC Studies of Interactions between ZnO-BPs and ZnO.** Thermodynamic binding experiments were carried out using a MicroCal VP-ITC Northampton, MA instrument by GE Healthcare. Interacting components were prepared in filtered ddH<sub>2</sub>O. In each experiment, the prepared peptide solution and the solution with suspended ZnO were degassed for 7 min using a Thermovac before loading in the ITC. Preliminary experiments were carried out to optimize the experimental conditions. The parameters chosen for the experiments were; temperature of 25

°C, a reference power of 15  $\mu\text{cal}/\text{sec}$ , syringe stirring speed of 394 rpm, a peptide concentration of 3.1 mM in a total volume of 280  $\mu\text{l}$  injected periodically in 10  $\mu\text{l}$  aliquots into the sample cell containing 1.4 ml ZnO suspension (0.1 mM  $\text{Zn}^{2+}$ ). At least 1000 sec was required in between injections to allow the baseline to return to equilibrium after each injection. A spacing of 1200 sec was required for the first 10 injections and a spacing of 1000 sec for the remaining 18 injections. In some experiments with GT-16, the spacing of the first 10 injections needed to be increased to 1600 sec. The heat effects measured in the peptide into water dilution experiments performed under identical timing of aliquot additions were subtracted from the heat effects of interaction (titration of peptide into ZnO suspension). Other dilution experiments performed were dilution of water into the cell containing the ZnO particles and the dilution of water into water which produced negligible heat measurements. Each experiment was at least duplicated. Data analysis was conducted using ORIGIN 7.0 software and fit using a non-linear least-squares algorithm with one set of sites and two sets of independent sites model from MicroCal.<sup>29</sup>

## RESULTS AND DISCUSSION

ITC experiments were carried out to measure heat effects taking place during the interaction of peptide with ZnO particles. The interactions were studied in aqueous media as in the synthesis studies.<sup>1,6,8</sup> Further information in support of the choice of media for ITC experiments is given in S1 of supporting information (SI). ITC experiments were designed to; (i) monitor heat effects of interaction between ZnO and the ZnO-BPs and identify the driving forces of interaction, (ii) determine if alanine mutants of G-12 had different thermodynamic signatures in their adsorption process compared to the original sequence, (iii) determine if differences in adsorption characteristics could be detected for different peptides with a single crystal morphology and an individual peptide with different crystal morphologies and (iv) possibly identify a direct link between thermodynamic changes that occur at the peptide-inorganic interface and the observed peptide directed structural modifications of ZnO.

**ITC Study of Interactions of G-12 and its Alanine Mutants with ZnO Rods.** ZnO solution synthesis studies with peptide had demonstrated that a single point mutation in G-12 sequence to form G-12A6 resulted in a drastic change in ZnO morphology, unlike with G-12A11 and G-12A12 (Figure 1).<sup>8</sup> Synthesis studies also showed that ZnO-BPs could strongly/irreversibly adsorb to ZnO.<sup>8</sup> Here, ITC was used to directly monitor the interaction of ZnO rods (48-hr precipitates obtained from synthesis using  $\text{Zn}(\text{NO}_3)_2 \cdot 6\text{H}_2\text{O}$  and HMTA) with G-12 and its alanine mutants (G-12A6, G-12A11 and G-12A12). The interactions produced measurable heat effects (Figure 1). With each peptide, two binding events occurred, an endothermic event followed by an exothermic event evidenced by positive and negative changes in differential power ( $Dp$ ) respectively. Peptide sequence dependent qualitative differences in the shapes of the isothermal profiles were observed.

Determination of surface coverage is important for quantification of binding potency and is also an indicator of whether monolayers or multilayers were formed.<sup>25,30</sup> In

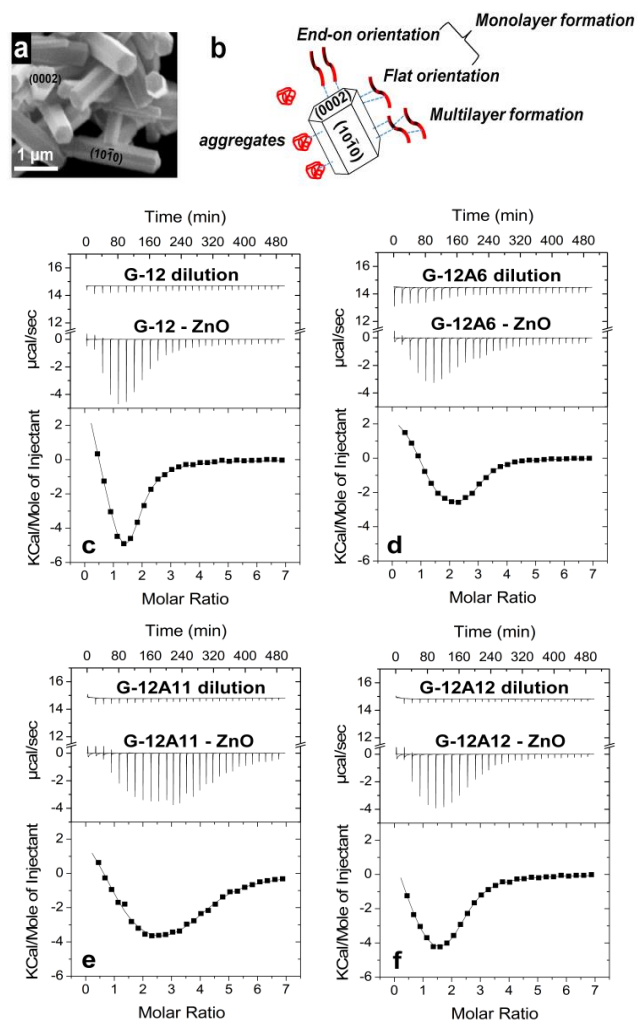


**Figure 1.** (a) SEM micrographs ZnO twinned rods,  $L/D = 8.92 \pm 3.26$  collected after 48 hrs of synthesis using the  $\text{Zn}(\text{NO}_3)_2 \cdot 6\text{H}_2\text{O}$  and HMTA system, (b) schematic representation of possible modes of interaction of peptide with ZnO surface (c-f) ITC isotherms showing heat effects measured in titration of G-12 and its alanine mutants G-12A6, G-12A11 and G-12A12 (3.1 mM) into suspensions of ZnO rods (0.1 mM bulk concentration). Dilution heat effect of titrating each peptide into water is also shown.

all the measured interactions, at least 100  $\mu\text{l}$  (at least 10 injections) of 3.1 mM peptide was needed to reach saturation. From estimation of the size of peptide molecules using molecular dynamics (MD) software, the theoretical maximum number of peptide molecules needed to form monolayer coverage (assuming that the peptides adsorbed to the ZnO surfaces end-on/upright for maximum possible monolayer coverage) on the total surface area of ZnO rods present in an ITC experiment (based on BET analysis), was less than the amount of peptide experimentally needed to attain saturation in ITC experiments. For example, the number of unit molecules of G-12 estimated to fill a monolayer was  $8.91 \times 10^{13}$  and the amount needed to reach saturation in ITC experiments was  $2.46 \times 10^{17}$ . In all the interactions, the amount of peptide needed to obtain saturation was in great excess of the amount required

to form monolayer coverage suggesting that dense peptide multilayers were formed on ZnO. It is for this reason

that normalized heat effects in kcal/mole of injectant were plotted against the molar ratio

**Table 1. Thermodynamic parameters obtained from ITC measurements of interaction of G-12 and its alanine mutants G-12A6, G-12A11 and G-12A12 (3.1 mM) with ZnO rods (0.1 mM bulk concentration). Temperature of 298 K was maintained throughout each experiment.  $\Delta S$  and  $\Delta G$  were calculated from  $\Delta H - T\Delta S = -RT\ln K_A = \Delta G$ .**

Peptide and ZnO	Dp	$K_A$ ( $M^{-1}$ )	$\Delta H$ (Kcal mol $^{-1}$ )	$T\Delta S$ (Kcal mol $^{-1}$ )	$\Delta G$ (Kcal mol $^{-1}$ )
G-12 - ZnO	+ve	$1.40 \times 10^6 \pm 0.33 \times 10^6$	$2.36 \pm 0.68$	$10.73 \pm 0.55$	$-8.37 \pm 0.13$
	-ve	$9.01 \times 10^4 \pm 0.32 \times 10^4$	$-7.55 \pm 1.09$	$-0.79 \pm 1.06$	$-6.76 \pm 0.02$
G-12A6 - ZnO	+ve	$2.65 \times 10^5 \pm 0.52 \times 10^5$	$5.47 \pm 3.12$	$12.86 \pm 3.22$	$-7.39 \pm 0.10$
	-ve	$6.79 \times 10^4 \pm 0.62 \times 10^4$	$-15.69 \pm 8.41$	$-9.09 \pm 5.79$	$-6.60 \pm 0.02$
G-12A11 - ZnO	+ve	$3.86 \times 10^5 \pm 2.14 \times 10^5$ *	$4.19 \pm 2.07$ *	$11.80$ *	$-7.61$ *
	-ve	$4.51 \times 10^4 \pm 0.47 \times 10^4$	$-6.69 \pm 1.22$	$-0.34 \pm 1.28$	$-6.34 \pm 0.06$
G-12A12 - ZnO	+ve	$4.47 \times 10^5 \pm 0.76 \times 10^5$	$5.74 \pm 0.76$	$13.42 \pm 0.86$	$-7.69 \pm 0.10$
	-ve	$8.58 \times 10^4 \pm 0.18 \times 10^4$	$-6.91 \pm 0.78$	$-0.55 \pm 0.25$	$-6.36 \pm 0.53$

(+ve) endothermic, (-ve) exothermic, (\*) designates parameters determined from one experiment, other parameters are an average of two measurements.

of the peptide concentration and the bulk concentration of ZnO determined from the dissolution study (performed using ICP- OES) even though the peptide would only interact with the surface of particles. It has been reported that the effective concentration of surface sites available for interaction ( $M_t'$ ) on particles can be estimated from adsorption studies (Langmuir adsorption isotherms) and BET determined surface area of the particles.<sup>31,32</sup> However, this may not be applicable in instances such as in this study where multilayer formation occurs with heat effects produced not only during monolayer adsorption. For the adsorption of G-12 and the selected alanine mutants to ZnO, the value  $M_t'$  would represent both the surface sites available on ZnO as well as the peptide binding sites that allow intermolecular interaction.

To determine the thermodynamic parameters of interaction, the heat effects of diluting peptide into water were first subtracted from the global observed heat effects ( $\Delta H_{obs}$ ) obtained during titration of the peptide into ZnO particles. Isotherms were then fitted using the two sets of independent binding sites model provided by MicroCal on the basis of the shape of the isotherm having two separate saturation events (Table 1). According to literature, the accuracy of determining the concentration of the syringe component in ITC experiments directly affects the accuracy of determining the parameters  $K_A$ , molar binding ratio ( $n$ ) and  $\Delta H$  whereas the accuracy of determining the concentration of the sample cell component only affects  $n$ .<sup>33</sup> As peptide concentration was known,  $K_A$  and  $\Delta H$  could be estimated but  $n$  was not defined because of the uncertainty of determining the concentration of surface binding sites on ZnO.

The interactions of the peptides with the different ZnO morphologies were favourable; based on the high ( $> 10^4 M^{-1}$ )<sup>21,34,35</sup> affinity values obtained and negative values of  $\Delta G$  which were estimated to lie in between -6 and -8.5 kcal/mol. These values were similar to those reported for the adsorption of fluorescent tagged EM-12 (and truncations of the sequence) to ZnO.<sup>20</sup> ITC is however a faster method that can directly probe thermodynamic parameters of interaction without the requirement for labelling or carrying out experiments at different concentrations or

temperatures to estimate thermodynamic parameters. In this study, the values of  $\Delta H$  and  $\Delta S$  were positive in all endothermic processes of the biphasic isotherms. The surfaces of many metal oxides like ZnO become hydroxylated in aqueous solution. The polar hydroxylated ZnO surface attracts and adsorbs water molecules which can either be chemisorbed or physisorbed.<sup>36</sup> As peptides moved towards the ZnO surface, peptide conformational changes as well as incorporation or displacement of water molecules may have occurred producing an endothermic heat effects with the largest contribution from positive values of  $\Delta S$ . Negative  $\Delta H$  values for the exothermic process indicated the occurrence of non-covalent interactions like hydrogen bonding, van der Waals forces or electrostatic interactions.<sup>26,27,37</sup> Although determination of changes in non-covalent interactions ( $K_A$ ,  $\Delta H$ ,  $\Delta S$ ) may not rigorously define interactions at an atomic scale, the information obtained may be a guideline towards understanding binding/adsorption processes.<sup>27</sup> As the amount of adsorbed peptide was greater than that needed to form monolayer coverage, the observed exothermic heat effect was attributed to contributions from both peptide-surface adsorption as well as peptide-peptide interactions. Two saturation events could have taken place; peptide saturation of the ZnO surface and peptide binding to peptide until peptide-peptide binding site saturation was achieved. The size of peptide molecules in solution measured using dynamic light scattering (DLS) ( $S_2$  of SI) suggests that a majority of the peptide molecules were in aggregated form in solution therefore peptide-peptide interactions could have already occurred and peptides could have adsorbed to the ZnO surface as aggregated entities. Therefore, it is possible that initial peptide-surface interaction could have also contributed to the observed endothermic heat effect together with conformational changes between free and bound peptide. Further peptide-peptide interaction could have then occurred characterised by the exothermic heat effect. There was therefore no stepwise process where a monolayer was first completed before multilayer formation; both processes would continue to occur simultaneously once further peptide-peptide interaction on peptide bound to

ZnO surface was initiated until saturation was reached. This may explain why stepwise saturation events usually associated with sequential multilayer adsorption was not observed. In support of this explanation, Lindman and co-workers reported multilayer adsorption of human serum albumin (HSA) to copolymer nanoparticles using ITC and similarly did not observe step-wise saturation events in isothermal profiles.<sup>25</sup>

The interaction of G-12A6, G-12A11 and G-12A12 with ZnO suggests that the respective alanine substitutions in G-12 sequence may have only caused localized changes in peptide structure which did not completely suppress binding potency. This may also suggest that interaction may be mediated by 'hot spot' regions rather than by a single amino acid. Unlike the other three peptides, dilution of G-12A6 into water resulted in a low heat signal which may be attributed to dissociation of peptide molecule aggregates that may have been present at higher peptide concentration in the syringe. This may be linked to the peptide's reported ability to template isotropic growth of ZnO in solution synthesis forming microspheres.<sup>8</sup> The concentration of G-12A11 needed to attain saturation was greater than the other three peptides. In G-12A11 (GLHVMHKVAPAR), P<sub>11</sub> of the original G-12 sequence was replaced with A<sub>11</sub>. The amino acid proline is known to have a restricted backbone conformation because its functional group is cyclised back against the backbone amide position.<sup>38</sup> G-12A11 was the only sequence without a proline-proline dipeptide at position 10 and 11 which may have significantly altered its conformation and packing density at saturation. The determined enthalpy change of the interaction of G-12 and mutants G-12A6, G-12A11 and G-12A12 with ZnO were similar but G-12 has a slightly greater affinity for the ZnO surface compared to the mutant sequences.

**ITC Study of Interactions of G-12 and GT-16 with ZnO Rods and Platelets.** ITC was also used to study the interaction of G-12 and GT-16 with two different morphologies of ZnO crystals; The 48-hr ZnO twinned rods from synthesis using the Zn(NO<sub>3</sub>)<sub>2</sub>·6H<sub>2</sub>O-HMTA system and ZnO twinned platelets similarly synthesized but also incorporating GT-16 peptide (Figure 2a, b). In comparison to ZnO rods, ZnO platelets had a greater surface area of the (0001) plane which GT-16 had been reported to preferentially adsorb to.<sup>6</sup> Previous studies using FTIR reported that the intermediate layered basic zinc nitrate (LBZN) was still present in the ZnO rods chosen for this study.<sup>8</sup> Here, using Raman spectroscopy, the symmetric N-O stretching vibration band at 1053 cm<sup>-1</sup> for NO<sub>3</sub><sup>-</sup> in LBZN was detected (Figure 2c). The LBZN in ZnO rods had been quantified using TGA to be 1.6 ± 0.2% of the total weight.<sup>28</sup> This amount was below XPS detection limit as nitrogen (N 1s peak) was not detected in the spectra of the ZnO rods (Figure 2d). The calculated relation of Zn/O was greater than 1 (Table 2) suggesting the presence of oxygen vacancies on the surface.<sup>28,39</sup> The amount of LBZN and peptide adsorbed to ZnO platelets was quantified (TGA) to be 7.5 ± 0.5%.<sup>28</sup> The strong adsorption of GT-16 to washed ZnO platelets was further confirmed from its Raman spectra by the presence of amide I (~1670 cm<sup>-1</sup>) band, amide III (~1300 cm<sup>-1</sup>) band and a peak arising from the

amino acid valine (~713 cm<sup>-1</sup>), all of which were also present in the spectra of GT-16 peptide (Figure 2c). XPS analysis confirmed the presence of GT-16 peptide on the surface of ZnO platelets by the detection of N 1s peak (Figure 2e, Table 2). The higher amount

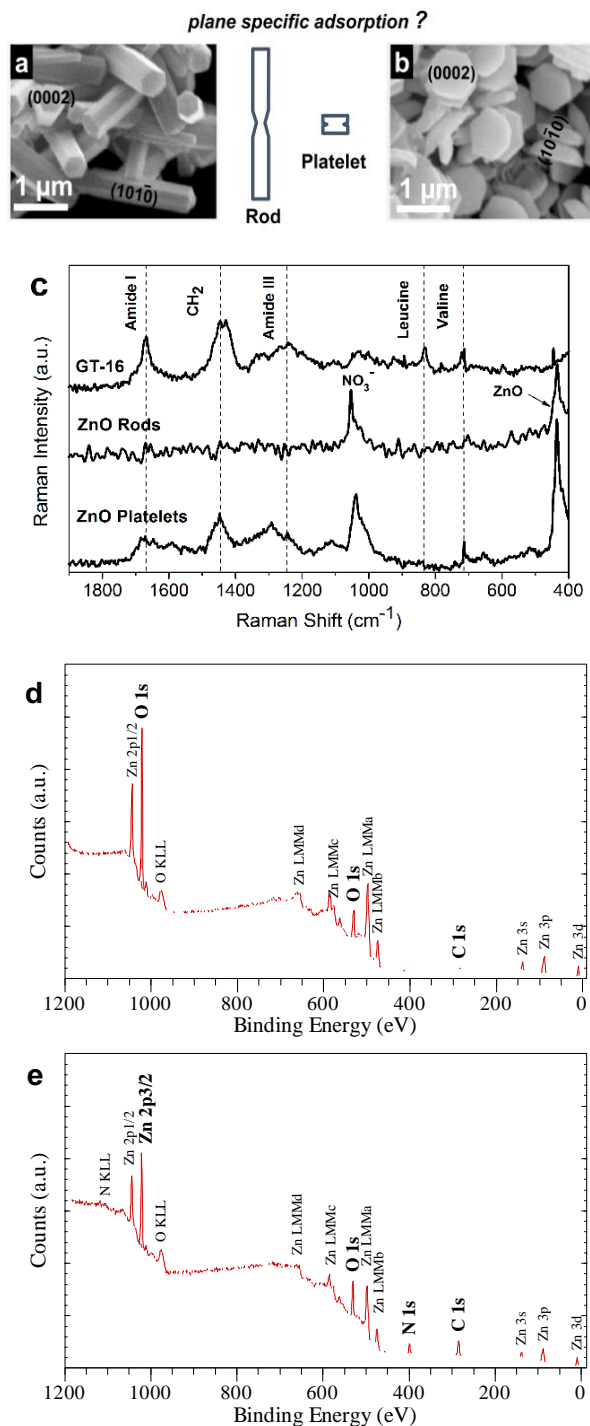


**Figure 2.** SEM micrographs (a) ZnO twinned rods, L/D = 8.92 ± 3.26 and (b) ZnO twinned platelets L/D = 0.69 ± 0.21 with schematic representations of the morphologies. (c) Raman spectra of the rods, platelets and GT-16 peptide. (d, e) XPS survey spectrum of the ZnO rods and platelets respectively.

**Table 2. XPS determined Atomic Percentage of C 1s, N 1s, Zn 2p<sub>3/2</sub> and O 1s peaks and the Relative Ratio of Zn/O**

ZnO Sample	% C	% N	% Zn	% O	Zn/O
Rods	7.1	-	48.6	44.3	1.1

Platelets	39.1	11.1	20.8	29.0	-
Rods calcined	8.4	-	52.3	39.3	1.3
Platelets calcined	15.6	-	43.2	41.2	1.0

Zn/O ratio for platelets not calculated as adsorbed peptide molecules contributed to the atomic percentage of O

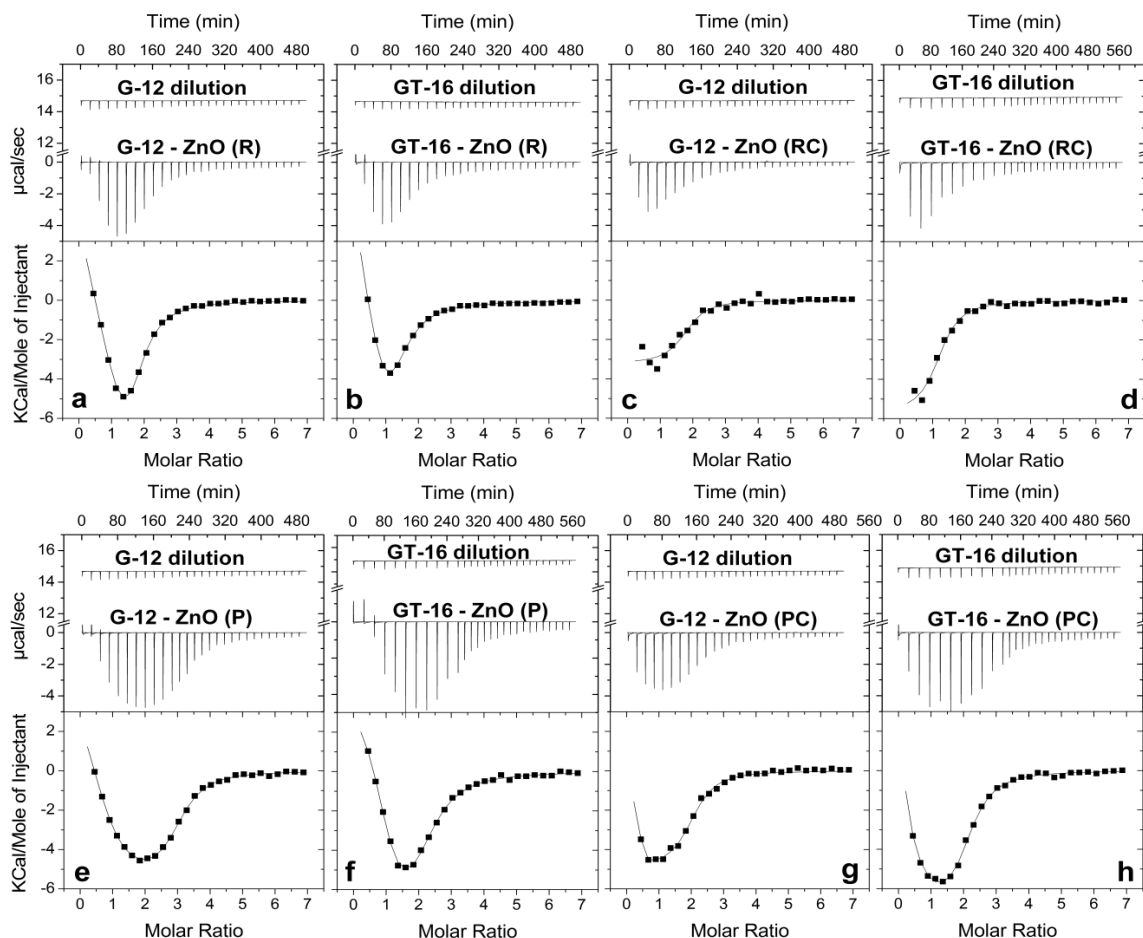


**Figure 3.** ITC isotherms representing heat effects of interaction measured in the titration of 3.1 mM G-12 and GT-16 into suspensions of ZnO rods (0.1 mM bulk concentration). ZnO morphologies have been designated; (R) rods, (RC) rods calcined, (P) platelets, (PC) platelets calcined. Titration of peptides into water to measure dilution heats is also shown.

**Table 3.** Thermodynamic parameters obtained from ITC measurements of interactions between 3.1 mM G-12 and GT-16 and 0.1 mM (bulk concentration) ZnO twinned rods/platelets. A constant cell temperature of 298 K was maintained. Entropy change and Gibbs free energy were calculated using the equation;  $\Delta H - T\Delta S = -RT\ln K_A = \Delta G$ .

Peptide and ZnO	Model	Dp	$K_A$ ( $M^{-1}$ )	$\Delta H$ (Kcal mol <sup>-1</sup> )	$T\Delta S$ (Kcal mol <sup>-1</sup> )	$\Delta G$ (Kcal mol <sup>-1</sup> )
G-12 - ZnO (R)	2	+ve	$1.40 \times 10^6 \pm 0.33 \times 10^6$	$2.36 \pm 0.68$	$10.73 \pm 0.55$	$-8.37 \pm 0.13$
		-ve	$9.01 \times 10^4 \pm 0.32 \times 10^4$	$-7.55 \pm 1.09$	$-0.79 \pm 1.06$	$-6.76 \pm 0.02$
GT-16 - ZnO (R)	2	+ve	$1.37 \times 10^5 \pm 2.52 \times 10^5$ *	$3.01 \pm 4.16$ *	$10.01$ *	$-7.00$ *
		-ve	$3.65 \times 10^4 \pm 3.12 \times 10^3$ *	$-3.06 \pm 0.21$ *	$3.16$ *	$-6.22$ *
G-12 - ZnO (RC)	1	-ve	$1.77 \times 10^5 \pm 0.33 \times 10^5$	$-3.07 \pm 0.21$	$4.08 \pm 0.34$	$-7.16 \pm 0.12$
GT-16 - ZnO (RC)	1	-ve	$1.31 \times 10^5 \pm 0.36 \times 10^5$	$-5.54 \pm 0.27$	$1.44 \pm 0.44$	$-6.97 \pm 0.17$
G-12 - ZnO (P)	2	+ve	$9.94 \times 10^5 \pm 2.98 \times 10^5$ *	$5.82 \pm 2.4$ *	$14.01$ *	$-8.19$ *
		-ve	$1.45 \times 10^5 \pm 0.21 \times 10^5$	$-6.18 \pm 0.16$	$0.85 \pm 0.25$	$-7.04 \pm 0.09$
GT-16 - ZnO (P)	2	+ve	$7.88 \times 10^5 \pm 2.93 \times 10^5$	$3.48 \pm 1.13$	$11.49 \pm 0.91$	$-8.01 \pm 0.22$
		-ve	$6.32 \times 10^4 \pm 0.97 \times 10^4$	$-9.42 \pm 0.16$	$-2.87 \pm 0.24$	$-6.55 \pm 0.08$
G-12 - ZnO (PC)	2	+ve	-	-	-	-
		-ve	$1.14 \times 10^5 \pm 0.13 \times 10^5$	$-4.76 \pm 0.36$	$2.14 \pm 0.28$	$-6.89 \pm 0.07$
GT-16 - ZnO (PC)	2	+ve	-	-	-	-
		-ve	$1.26 \times 10^5 \pm 0.04 \times 10^5$	$-8.23 \pm 0.44$	$-1.27 \pm 0.41$	$-6.95 \pm 0.02$

R) rods, (RC) rods calcined, (P) platelets, (PC) platelets calcined, (+ve) endothermic, (-ve) exothermic, (1) one set of sites model, (2) two sets of sites model. Data is an average of at least two measurements, however in some experiments designated

(\*), only one experiment gave reasonable values after fitting, (-) values not calculated as very few data points were obtained in the particular region needed for analysis.

---

of Carbon (C 1s peak) detected in ZnO platelets in comparison to that in ZnO rods could also be attributed to peptide adsorption rather than adventitious carbon (Table 2). There was no evidence of peptide incorporation into the lattice of ZnO platelets by a comparison of d-spacing values (XRD) for the (10 $\bar{1}$ 0) plane (for growth along the a-axis) and the (0001) plane (for growth along c-axis) of ZnO rods against the platelets.<sup>8</sup> Thus adsorption studies with ZnO platelets would be characterizing a peptide-peptide adsorption process. ITC experiments were therefore carried out with the particle as directly obtained from solution synthesis and after calcination to 900 °C to remove adsorbed molecules (chemisorbed water, LBZN and peptide where present). XPS survey spectra of calcined ZnO rods and platelets is shown in Figure S3 of SI and the atomic percentages of C 1s, Zn 2p<sub>3/2</sub> and O 1s peaks as well as the relative ratio of Zn/O in Table 2.

Qualitative differences in binding isotherms could be identified when interactions of both peptides (G-12 and GT-16) with the same particles (either rods or platelets, calcined or non-calcined) or the same peptide with different particles was compared (Figure 3). Interestingly, longer time spacing in between injections was needed with GT-16 for the heat effect per injection to return to thermal equilibrium (back to the baseline) compared to G-12. GT-16 may have required longer time to attain its stable binding conformation. This was observed with all the particles except the non-calcined ZnO rods. More injections, hence higher peptide concentration was required to saturate the same mass of ZnO platelets compared to ZnO rods which had a lower surface area available for interaction. Calcination of ZnO caused physico-chemical changes on the surface *i.e.* removal of chemisorbed water and peptide. These differences are reflected in the changes in the isothermal profiles; the characteristic endothermic and exothermic heat effect of the interaction were still observed but a shift of the isotherm to the right demonstrated that calcination caused changes to the ZnO surface, affecting interactions at the interface that could be distinguished by the instrument. Depending on the shape of the isotherm, data was fit using either the one or two sets of binding sites model provided by MicroCal (Table 3). Once again, the endothermic process, supported by positive values of  $\Delta S$  and  $\Delta H$ , was attributed to displacement of water, peptide conformational changes and possibly also initial peptide-surface interaction. The exothermic process was attributed to the occurrence of peptide-surface as well as peptide-peptide interactions driven by non-covalent forces. The affinity of G-12 for non-calcined ZnO rods and platelets appeared to be slightly greater than the affinity of GT-16 however for the calcined crystals the peptides had similar affinity. It was difficult to establish a clear difference in the interaction of GT-16 with the two crystal morphologies that could directly be correlated to the preferential adsorption of GT-16 to (0001) plane. Here, the peptides were exposed to interaction with whole crystals as opposed to single crystalline films as in the previous study demonstrating preferential adsorption of GT-16 to (0001)

plane.<sup>6</sup> With whole crystals, GT-16 adsorbs to the (0001) plane but is also able to adsorb to the (10 $\bar{1}$ 0) plane of ZnO. The likely simultaneous occurrence of peptide-surface and peptide-peptide interactions and the formation of multilayers could have also masked detection of differences in adsorption thermodynamics of the ZnO-BPs examined with the same or different crystal morphologies/surfaces. It has been reported that where peptide-peptide interactions take place forming multilayers, adsorption energies of single peptides can greatly be diminished.<sup>40</sup> Thus, for this system a direct link between thermodynamic changes and the differences observed in morphology modification in the presence of peptides was difficult to obtain. However, ITC allowed direct characterization of ZnO-ZnO-BP interactions and the quantification of energetic changes occurring during the adsorption process.

It is interesting to note that for the phage display identified peptides, when bound to phages during selection, their ability to form intermolecular interactions and aggregate is restricted. Conversely, artificially synthesized peptides free in solution are able to aggregate through peptide-peptide interactions depending on the amino acid residues present and solution conditions. Nevertheless, these artificially synthesized peptides are still able to interact with the material they were selected against in phage display experiments, though there may be some differences in their interaction. For single chain peptides or aggregated peptides, their interaction with the target surface is dependent on whether they are in a conformation such that the active binding site/important residue (or group of residues), in the 'hot spot' for interaction is available for interaction. Further studies are needed to fully understand the structure of the peptides (single chains, aggregated forms and the effects of the extent of aggregation). More information is needed to define the binding sites on the peptide and the inorganic surface to account for conformational changes including deaggregation of peptide in order to build models that are more representative of the interaction process. In using the one set of identical sites model and two sets of independent sites model, our objective was to fit the data with preferably the fewest adjustable parameters which is synonymous to selecting the simplest binding model that can be used to describe the process.<sup>41,42</sup> Nevertheless, there are practical difficulties in using these models to fit data for such complex systems as demonstrated in Figure S4 and S5 of SI. More representative and standardized mathematical models can be formulated if additional similar studies are carried out on different material and peptide combinations.

Moreover, as combinatorial methods such as phage display technique have known intrinsic biases associated with their use, development of other complementary approaches for identification and selection of specific material binding peptides are to be encouraged.<sup>43-45</sup> Molecular simulation techniques allow for theoretical investigation of the behaviour of complex systems at a molecular level

beyond what can presently be achieved experimentally.<sup>46,47</sup> Information obtained from ITC studies can be used to improve computational simulation strategies and validate the design of force fields to more accurately describe peptide-peptide and peptide-inorganic interactions. Furthermore, we propose the use of ITC as a screening method to distinguish between strong and weak binders by determining peptide affinity for target substrates. This may be particularly clear where adsorption processes are saturated within or close to monolayer coverage. Much progress is needed to accelerate the rationale used to identify inorganic binding peptides with integrated properties and functionality.

## CONCLUSIONS

Using ITC, the interaction of ZnO and ZnO-BPs has been shown to occur through a biphasic process involving and endothermic and exothermic event. High adsorption affinity values indicated the occurrence of favourable interactions with  $\Delta G$  values between -6 and -8.5 kcal/mol. The adsorption of the ZnO-BPs was seen to be a process involving simultaneous interactions *i.e.* peptide-solvent, substrate-solvent, peptide-surface, possible conformation changes between bound and free peptide states and peptide-peptide interactions. The wider use of ITC to study other peptide-inorganic interaction systems, in combination with other conventional techniques used to kinetically/thermodynamically characterize peptide-inorganic interactions may collectively build knowledge that can enable control over material formation processes to be achieved, mastered and exploited to advance material design processes. Though the use of ITC to monitor biotic-abiotic interactions has its challenges, with continued improvements in instrumentation, methodology and binding models, its development for novel applications is far from being exhausted.

## ASSOCIATED CONTENT

**Supporting Information.** Text S1, Figure S2 to S5. This material is available free of charge *via* the Internet at <http://pubs.acs.org>.

## AUTHOR INFORMATION

### Corresponding Author

\* Email: Carole.Perry@ntu.ac.uk

### Author Contributions

All authors have given approval to the final version of the manuscript.

### Funding Sources

U.S. Air Force Office of Scientific Research (AFOSR) for funding (FA9550-10-1-0024) and (FA9550-13-1-0040).

### Notes

The authors declare no competing financial interest.

## ACKNOWLEDGMENT

We would like to thank Dr. Graham J. Hickman for performing mass spectrometry analysis of the peptides studied, Dr. David J. Belton for the surface area measurements of ZnO particles, Anna Sola-Rabada and Mr. Martin J. Roe (Advanced Materials Research Group, X-ray Photoelectron Spectroscopy, Faculty of Engineering, The University of Notting-

ham) for the X-ray photoelectron spectroscopy analysis of ZnO particles. We are grateful to the U.S. Air Force Office of Scientific Research (AFOSR) for funding this fundamental research study.

## REFERENCES

- (1) Tomczak, M. M.; Gupta, M. K.; Drummy, L. F.; Rozenzhak, S. M.; Naik, R. R. Morphological Control and Assembly of Zinc Oxide Using a Biotemplate. *Acta Biomater.* **2009**, *5*, 876–882.
- (2) Chiu, C. Y.; Li, Y.; Ruan, L.; Ye, X.; Murray, C. B.; Huang, Y. Platinum Nanocrystals Selectively Shaped Using Facet-specific Peptide Sequences. *Nature Chemistry* **2011**, *3*, 393–399.
- (3) Chiu, C.; Ruan, L.; Huang, Y. Biomolecular Specificity Controlled Nanomaterial Synthesis. *Chem. Soc. Rev.* **2013**, *42*, 2512–2527.
- (4) Ruan, L.; Ramezani-Dakhel, H.; Chiu, C.; Zhu, E.; Li, Y.; Heinz, H.; Huang, Y. Tailoring Molecular Specificity Toward a Crystal Facet: a Lesson From Biorecognition Toward Pt {111}. *Nano Lett.* **2013**, *13*, 840–846.
- (5) Togashi, T.; Yokoo, N.; Umetsu, M.; Ohara, S.; Naka, T.; Takami, S.; Abe, H.; Kumagai, I.; Adschiri, T. Material-binding Peptide Application – ZnO Crystal Structure Control by Means of a ZnO-binding Peptide. *J. Biosci. Bioeng.* **2011**, *111*, 140–145.
- (6) Liang, M.; Deschaume, O.; Patwardhan, S. V.; Perry, C. C. Direct Evidence of ZnO Morphology Modification via the Selective Adsorption of ZnO-binding Peptides. *J. Mater. Chem.* **2011**, *21*, 80–89.
- (7) Baier, J.; Naumburg, T.; Blumenstein, N. J.; Jeurgens, L. P.; Welzel, U.; Do, T. A.; Pleiss, J.; Bill, J. Bio-inspired Mineralization of Zinc Oxide in Presence of ZnO-binding Peptides. *Biointerface Res. Appl. Chem.* **2012**, *2*, 380–391.
- (8) Limo, M. J.; Ramasamy, R.; Perry, C. C. ZnO Binding Peptides: Smart Versatile Tools for Controlled Modification of ZnO Growth Mechanism and Morphology. *Chem. Mater.* **2015**, *27*, 1950–1960.
- (9) Brown, S.; Sarikaya, M.; Johnson, E. A Genetic Analysis of Crystal Growth. *J. Mol. Biol.* **2000**, *299*, 725–735.
- (10) Slocik, J. M.; Stone, M. O.; Naik, R. R. Synthesis of Gold Nanoparticles Using Multifunctional Peptides. *Small* **2005**, *1*, 1048–1052.
- (11) Kim, J.; Rheem, Y.; Yoo, B.; Chong, Y.; Bozhilov, K. N.; Kim, D.; Sadowsky, M. J.; Hur, H.; Myung, N. V. Peptide-mediated Shape- and Size-tunable Synthesis of Gold Nanostructures. *Acta Biomater.* **2010**, *6*, 2681–2689.
- (12) Chiu, C.; Li, Y.; Huang, Y. Size-controlled Synthesis of Pd Nanocrystals Using a Specific Multifunctional Peptide. *Nanoscale* **2010**, *2*, 927–930.
- (13) Xie, J.; Lee, J. Y.; Wang, D. I.; Ting, Y. P. Silver Nanoplates: from Biological to Biomimetic Synthesis. *ACS Nano* **2007**, *1*, 429–439.
- (14) Patwardhan, S. V.; Patwardhan, G.; Perry, C. C. Interactions of Biomolecules with Inorganic Materials: Principles, Applications and Future Prospects. *J. of Mater. Chem.* **2007**, *17*, 2875–2884.
- (15) Whyburn, G. P.; Li, Y. J.; Huang, Y. Protein and Protein Assembly Based Material Structures. *J. of Mater. Chem.* **2008**, *18*, 3755–3762.
- (16) Cedervall, T.; Lynch, I.; Lindman, S.; Berggård, T.; Thulin, E.; Nilsson, H.; Dawson, K. A.; Linse, S. Understanding the Nanoparticle-Protein Corona Using Methods to Quantify Exchange Rates and Affinities of Proteins for Nanoparticles. *Proc. Natl. Acad. Sci.* **2007**, *104*, 2050–2055.
- (17) Perry, C. C.; Patwardhan, S. V.; Deschaume, O. From Biominerals to Biomaterials: the Role of Biomolecule-Mineral Interactions. *Biochem. Soc. Trans.* **2009**, *37*, 687–691.

- (18) Sola-Rabada, A.; Liang, M.; Roe, M. J.; Perry, C. C. Peptide-directed crystal growth modification in the formation of ZnO. *J. Mater. Chem. B* **2015**, *3*, 3777–3788.
- (19) Masuda, Y.; Kinoshita, N.; Koumoto, K. Morphology Control of ZnO Crystalline Particles in Aqueous Solution. *Electrochim. Acta* **2007**, *53*, 171–174.
- (20) Yokoo, N.; Togashi, T.; Umetsu, M.; Tsumoto, K.; Hattori, T.; Nakanishi, T.; Ohara, S.; Takami, S.; Naka, T.; Abe, H.; Kumagai, I.; Adschiri, T. Direct and Selective Immobilization of Proteins by Means of an Inorganic Material-Binding Peptide: Discussion on Functionalization in the Elongation to Material-Binding Peptide. *J. Phys. Chem. B* **2010**, *114*, 480–486.
- (21) Okochi, M.; Sugita, T.; Furusawa, S.; Umetsu, M.; Adschiri, T.; Honda, H. Peptide Array-based Characterization and Design of ZnO-high Affinity Peptides. *Biotechnol. Bioeng.* **2010**, *106*, 845–851.
- (22) Rothenstein, D.; Claasen, B.; Omiecinski, B.; Lammel, P.; Bill, J. Isolation of ZnO-binding 12-mer Peptides and Determination of their Binding Epitopes by NMR Spectroscopy. *J. Am. Chem. Soc.* **2012**, *134*, 12547–12556.
- (23) Lynch, I.; Dawson, K. A. Protein-Nanoparticle Interactions. *Nano Today* **2008**, *3*, 40–47.
- (24) Huang, R.; Carney, R.; Stellacci, F.; Lau, B. Protein-Nanoparticle Interactions: The Effects of Surface Compositional and Structural Heterogeneity is Scale Dependent. *Nanoscale* **2013**, *5*, 6928–6935.
- (25) Lindman, S.; Lynch, I.; Thulin, E.; Nilsson, H.; Dawson, K. A.; Linse, S. Systematic Investigation of the Thermodynamics of HSA Adsorption to N-iso-propylacrylamide/N-tert-butylacrylamide Copolymer Nanoparticles. Effects of Particle Size and Hydrophobicity. *Nano Lett.* **2007**, *7*, 914–920.
- (26) Ababou, A.; Ladbury, J. E. Survey of the Year 2004: Literature on Applications of Isothermal Titration Calorimetry. *J. Mol. Recognit.* **2006**, *19*, 79–89.
- (27) Cliff, M. J.; Gutierrez, A.; Ladbury, J. E. A Survey of the Year 2003 Literature on Applications of Isothermal Titration Calorimetry. *J. Mol. Recognit.* **2004**, *17*, 513–523.
- (28) Liang, M.; Limo, M. J.; Rabada, A. S.; Roe, M.; Perry, C. C. New Insights into the Mechanism of ZnO Formation from Aqueous Solutions of Zinc Acetate and Zinc Nitrate. *Chem. Mater.* **2014**, *26*, 4119–4129.
- (29) MicroCal, L. ITC Data Analysis in Origin Tutorial Guide; Northampton, MA, USA, **2004**.
- (30) Cohavi, O.; Reichmann, D.; Abramovich, R.; Tesler, A. B.; Bellapadrona, G.; Kokh, D. B.; Wade, R. C.; Vaskevich, A.; Rubinstein, I.; Schreiber, G. A Quantitative, Real-Time Assessment of Binding of Peptides and Proteins to Gold Surfaces. *Chem. Eur. J.* **2011**, *17*, 1327–1336.
- (31) Goobes, G.; Goobes, R.; Shaw, W. J.; Gibson, J. M.; Long, J. R.; Raghunathan, V.; Schueler-Furman, O.; Popham, J. M.; Baker, D.; Campbell, C. T. The Structure, Dynamics, and Energetics of Protein Adsorption – Lessons Learned from Adsorption of Statherin to Hydroxyapatite. *Magn. Reson. Chem.* **2007**, *45*, S32–S47.
- (32) Goobes, R.; Goobes, G.; Shaw, W. J.; Drobny, G. P.; Campbell, C. T.; Stayton, P. S. Thermodynamic Roles of Basic Amino Acids in Statherin Recognition of Hydroxyapatite. *Biochemistry* **2007**, *46*, 4725–4733.
- (33) Myszka, D.; Abdiche, Y.; Arisaka, F.; Byron, O.; Eisenstein, E.; Hensley, P.; Thomson, J.; Lombardo, C.; Schwarz, F.; Stafford, W.; Doyle, M. L. The ABRF-MIRG'02 Study: Assembly State, Thermodynamic, and Kinetic Analysis of an Enzyme/Inhibitor Interaction. *J. Biomol. Tech.* **2003**, *14*, 247.
- (34) Chiad, K.; Stelzig, S. H.; Gropeanu, R.; Weil, T.; Klapper, M.; Mullen, K. Isothermal Titration Calorimetry: A Powerful Technique to Quantify Interactions in Polymer Hybrid Systems. *Macromol.* **2009**, *42*, 7545–7552.
- (35) Bouchemal, K.; Mazzaferro, S. How to Conduct and Interpret ITC Experiments Accurately for Cyclodextrin–Guest Interactions. *Drug Discov. Today* **2012**, *17*, 623–629.
- (36) Degen, A.; Kosec, M. Effect of pH and Impurities on the Surface Charge of Zinc Oxide in Aqueous Solution. *J. Eur. Ceram. Soc.* **2000**, *20*, 667–673.
- (37) Leavitt, S.; Freire, E. Direct Measurement of Protein Binding Energetics by Isothermal Titration Calorimetry. *Curr. Opin. Struct. Biol.* **2001**, *11*, 560–566.
- (38) Williamson, M. P. The Structure and Function of Proline-rich Regions in Proteins. *Biochem. J.* **1994**, *297*, 249–260.
- (39) Zheng, Y.; Chen, C.; Zhan, Y.; Lin, X.; Zheng, Q.; Wei, K.; Zhu, J.; Zhu, Y. Luminescence and Photocatalytic Activity of ZnO Nanocrystals: Correlation between Structure and Property. *Inorg. Chem.* **2007**, *46*, 6675–6682.
- (40) Coppage, R.; Slocik, J. M.; Briggs, B. D.; Frenkel, A. I.; Naik, R. R.; Knecht, M. R. Determining Peptide Sequence Effects That Control the Size, Structure, and Function of Nanoparticles. *ACS Nano* **2012**, *6*, 1625–1636.
- (41) Schmidtchen, F. P. Isothermal Titration Calorimetry in Supramolecular Chemistry. In *Analytical methods in supramolecular chemistry*; Wiley VCH, **2012**, 67–103.
- (42) Limo, M. J.; Perry, C. C.; Thyparambil, A.; Wei, Y.; Latour, R. A. In *Experimental Characterization of Peptide–Surface Interactions*; Bio-Inspired Nanotechnology; Springer, **2014**, 37–94.
- (43) Puddu, V.; Perry, C. C. Peptide Adsorption on Silica Nanoparticles: Evidence of Hydrophobic Interactions. *ACS Nano* **2012**, *6*, 6356–6363.
- (44) Vodnik, M.; Zager, U.; Strukelj, B.; Lunder, M. Phage Display: Selecting Straws Instead of a Needle from a Haystack. *Molecules* **2011**, *16*, 790–817.
- (45) Slocik, J. M.; Naik, R. R. Probing Peptide–Nanomaterial Interactions. *Chem. Soc. Rev.* **2010**, *39*, 3454–3463.
- (46) Di Felice, R.; Corni, S. Simulation of Peptide–Surface Recognition. *J. Phys. Chem. Lett.* **2011**, *2*, 1510–1519.
- (47) Pandey, R. B.; Heinz, H.; Feng, J.; Farmer, B. L.; Slocik, J. M.; Drummy, L. F.; Naik, R. R. Adsorption of Peptides (A<sub>3</sub>, Flg, Pd<sub>2</sub>, Pd<sub>4</sub>) on Gold and Palladium Surfaces by a Coarse-grained Monte Carlo Simulation. *Phys. Chem. Chem. Phys.* **2009**, *11*, 1989–2001.

